Electrical Power and Energy Systems 156 (2024) 109697

Contents lists available at ScienceDirect

International Journal of Electrical Power and Energy Systems

journal homepage: www.elsevier.com/locate/ijepes

An adaptive voltage control compensator for converters in DC microgrids under fault conditions

Meysam Yadegar [a], Seyed Fariborz Zarei [a,*], Nader Meskin [b], Ahmed Massoud [b]

[a] Department of Electrical and Computer Engineering, Qom University of Technology, Qom, Iran
[b] Department of Electrical Engineering, Qatar University, Doha, Qatar

ARTICLE INFO

Keywords:
DC microgrids
Fault conditions
Fault-tolerant control
Voltage compensator
Multi-converter microgrid

ABSTRACT

This paper proposes a voltage compensator for converters in multi-converter DC microgrids (MG), which enhances the DC-MG behavior under fault conditions. Among the four existing categories in the classification of the faults, this paper focuses on those faults that affect voltage generation of converter-based distributed generation units (DGUs). Such faults conceptually occur from the terminal voltage reference to actual voltage generated by DGUs. To compensate the adverse effects of the faults, an adaptive scheme is proposed, which considers the most general case of the faults by using the time-varying multiplicative and additive fault models. The proposed scheme benefits from an integrated structure, which does not require separate fault detection, isolation, and identification blocks. As an advantage of the proposed approach, it is designed independent of the primary and secondary controllers of DGUs, and hence its performance is not affected by using different primary and secondary controllers. The effectiveness of the proposed scheme is verified under various fault conditions and uncertainty in the system parameters. Using the proposed scheme, the results show that the performance of system under the fault condition is similar to that of the normal operation.

1. Introduction

The use of various DC electronic loads, emerging DC energy sources, incorporation of energy storage systems into the electrical grid in one side, and various operational advantageous of using the DC electricity are the motivations toward implementing the DC microgrids. DC microgrid is a power cluster of DC loads, DC sources, and energy storage devices. All these elements have power electronic converter-based interfaces, which provide high efficiency and controllability.

In DC microgrid, the converter-interfaced distributed generation units (DGUs) have critical role, which control/regulate the voltage of the DC microgrid by their various control layers. In this respect, different hierarchical control levels are employed to define the different necessary Refs. [1,2]. The first inner level consists of voltage and current loops, which provides output voltage and current controllability for each DC source in the microgrid. The second control layer determines the power sharing among each DC sources and it can be divided into three schemes of (i) decentralized secondary control, (ii) distributed secondary control, and (iii) centralized secondary control [3].

Despite different advantages of DGU control system, they may face by different operational challenges, and accordingly, proper solutions have to be developed. The operation under fault condition is one of the most important issues, which is the main focus of this paper. The term *fault* can be used for description of various abnormal conditions, and variety of fault types are introduced till today [4–6]. In recent years, development of fault diagnosis and the associated "fault tolerant control" schemes have attracted researcher's attention in different fields [7–9].

By analyzing the faults in the power electronic converter-based systems, the different fault conditions and the associated fault tolerant control schemes are summarized in Table 1. In this table, we have classified the probable faults into four categories of "A"-to-"D" with fault cases of "F_1"-to-"F_7". It is worth to note that only "non-severe" faults are considered, as the "severe" faults are removed by protection systems, and control system is not involved for compensation of the "severe" faults. For more clarification, Fig. 1 shows the schematic diagram of a DC microgrid with multiple DGUs, focusing on the various probable faults in the different elements of the system. As shown in Fig. 1(a), the physical location of faults is indicated by "F_1" to "F_7" in the power circuit diagram representation form. Furthermore, Fig. 1(b) shows the faults location in the control diagram representation form. As shown in this figure, the faults "F_1" to "F_7" are classified into four categories of A-to-D considering their impact on the control system. In other words, the categories "A"-to-"D" show that how each fault affects the control system of the DC-microgrid. More details are provided in the following subsections.

* Corresponding author.
E-mail address: zarei@qut.ac.ir (S.F. Zarei).

https://doi.org/10.1016/j.ijepes.2023.109697
Received 7 April 2023; Received in revised form 11 November 2023; Accepted 30 November 2023
Available online 8 December 2023
0142-0615/

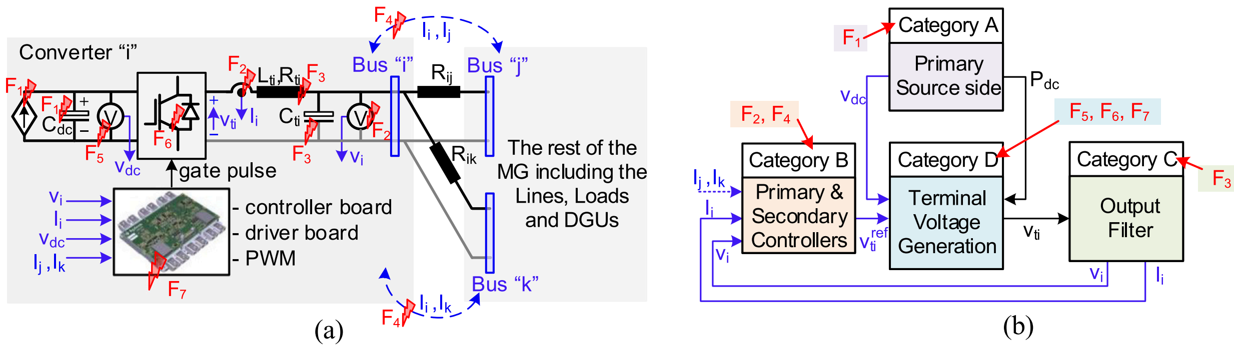

Fig. 1. Schematic diagram of a DC microgrid with multiple DGUs, focusing on the various probable faults in the different elements of a DGU, (a) faults F_1 to F_7 location in power circuit diagram representation form, (b) faults F_1 to F_7 location in control diagram representation form.

Table 1
The classification of faults and the relevant works in the literature.

Category	Fault	Solution	References
A	F1	Compensation by control action	[10–13]
B	F2 F4	Fault tolerant control scheme Fault tolerant control scheme	[14–21] [22–26]
C	F3	Control compensation	[27,28]
D	F5 F6 F7	Fault tolerant control scheme	**This paper**

1.1. Category A: Primary source side

This category considers variety of the faults which affect the primary source-side of DGU. Such faults include faults on DC-bus, the DC-link capacitor, and the primary DC-source, modeled by F_1 in Fig. 1(a).

The severe F_1 faults are mainly caused either by physical damages or by electrical faults of short circuits and over-voltages. Such faults are destructive and should be suppressed quickly by proper protective devices. Despite the severe faults, non-severe faults can be compensated using proper control actions. An FTC based on fuzzy logic and model predictive control for compensation of power-loss malfunction in the solar photovoltaic system (PVS) [10], the shading fault detection in PVS [11], a hierarchical-based FTC for sub-module (SM) level/phase level/bus level fault detection [12], a data-driven-based method for detection of hot spots in photovoltaic systems [13] are some examples of studies in this topic.

1.2. Category B: Primary and secondary controllers

This category includes all the faults which affect the functionality of the primary and secondary controllers in DGU. Generally, the root cause of such faults are external with respect to the primary and secondary controllers. The erroneous/inaccurate measurement of the sensors (F_2 in Fig. 1(a)) and the inaccurate/false data obtained by communication network (F_4 in Fig. 1(a)) are the main reasons for such faults. Couple of research works are available in this subject area, which are reviewed in the following.

Severe sensor faults are mainly caused by broken connectors and aging of electronic circuit components [29]. Such faults require replacement of the sensors, which demands the converter trip. Under severe communication network fault conditions, the data packets are lost, and the control system has to switch to the local control mode operation [30].

Compared to severe faults, the non-severe faults can be compensated by proper FTC schemes. Various FTC-based approaches are available in the literature which consider sensor and communication faults. Distributed observer-based H_∞ FTC [14], sliding mode observer-based FTC [15], FTC based on sliding mode control [16], FTC based on virtual sensor and Takagi–Sugeno (TS) model [17], FTC based on Back-stepping control [18], adaptive FTC [19], FTC based on the optimal PI controller [20], and FTC based on FDI [21] are examples of FTC-based studies against sensor faults. Furthermore, FTC based on sliding mode control [22], FTC based on the input–output feedback linearization technique [23], and FTC based on online recursive reduced-order estimation [24], decentralized consensus decision-making-based method [25], voltage distributed cooperative control scheme considering communication security [26], are some FTC schemes against communication faults.

1.3. Category C: Output filter

This category considers the faults affecting the output filter inductor and capacitor as shown by F_3 in Fig. 1(a). This fault also can be either severe or non-severe. The severe fault condition occurs due to insulation failure and physical damages on devices. The copper wire insulation deficiency, turn-to-grounded framework fault, and turn-to-turn faults are samples of severe faults on inductor. The capacitor failure and its fuse burnout are the examples of severe fault on filter capacitor. Such faults should be removed by the protective devices, and the converter trip is required in response to the fault. The values of filter inductance and capacitance are changed as time goes by during the operation [27]. Such drifts on the values can be considered as non-severe faults on output filters. Under non-severe fault conditions, controllers should detect/estimate/compensate the changes [28].

1.4. Category D: Terminal voltage generation

This category collects all the faults that affect the terminal voltage generation of DGU. More clearly, the faults occurring from the terminal voltage reference obtained by controllers to the actual terminal voltages generated by the DGU belong to this category. Such faults include the faults at DC-link voltage sensor, the power electronic switches, the controller board, the driver board, pulse-width modulation (PWM), and etc. These faults, as schematically shown by F_5, F_6 and F_7 in Fig. 1(a), can be either severe or non-severe faults. Under severe fault condition, the fault should be detected and proper action is required. Various studies are done in this topic such as SC detection [31], SC and open-circuit (OS) monitoring [32], reliability enhancement under SC condition [33], aging monitoring based on the SC current [34], and OC failure detection [35], and etc.

Non-severe faults of this category can be caused by the nuisance operation of DC-link voltage sensor, the errors on analog circuits of pulse transmission, mal-operation or nuisance operation of driver board, mal-operation of IGBTs and Diodes due to increase of parasitic characteristics by aging, and etc. Such faults do not require any immediate isolation actions, and proper fault tolerant control schemes may help to enhance the functionality of the DGU. To the best of the authors knowledge, the development of FTC scheme for non-severe faults of Category D has not been considered in the previous works in the literature.

1.5. Key contributions of the paper

With refer to the existing studies summarized in Table 1, and to the best of the authors' knowledges, the non-severe faults of Category D have not been studied yet in the literature. This fault category includes the fault locations of "F_5", "F_6", and "F_7", which directly affect the generated voltages of the power converters. To fill this gap, this paper focuses on this category of fault, and accordingly, an adaptive FTC is proposed.

On the other hand, the proposed FTC has some main distinctions with respect to other FTC methods for other classes of faults reported in the literature. For example, the approaches in [15–17,22–24] need a separate fault detection, isolation and identification units (FDI) that give the exact information about the place and the severity of the fault. Therefore, fault estimation error can affect the performance of FTC, specially in non-severe faults, while the proposed FTC does not require it. Furthermore, the design procedure of FTC in [18–20,36,37], for example, is based on the nominal primary/secondary controller. Therefore, if the nominal primary/secondary controller is changed, then FTC should be redesigned. While, the controller design steps of the proposed FTC is independent of the nominal primary/secondary controller.

The followings are the main contributions and goals of the study:

1. The proposed adaptive FTC scheme is dedicated to operate against the non-severe faults of Category D.
2. Faults in Category D are modeled by the most general format of time-varying multiplicative and additive factors.
3. The effective compensation against the Category D faults is the main goal/achievement of the proposed FTC scheme, and the results prove that the proposed scheme provides normal operating condition in the presence of faults.
4. Using the proposed FTC scheme, it is not required to modify the prevalent control structure of DC-microgrid and also the primary/secondary controllers of the DGUs. In other words, the proposed controller is designed independent from internal primary/secondary controller of DGUs.
5. A separate fault detection, isolation and identification units are not used in the proposed FTC scheme.

It is noted that the other type of faults such as sensor faults are out of scope of this paper.

The structure of the paper is organized as follows. Section 2 provides the necessary background and elaborates the problem formulation. The controller design steps of the proposed adaptive FTC scheme is explained in Section 3. To illustrate the effectiveness of the proposed FTC, various scenarios and obtained results are given in Section 4. Section 5 provides the conclusion. Finally, Some preliminaries and the proof of a theorem and a proposition presented in the paper are provided in Appendices B–C.

2. Background and problem formulation

2.1. Notations

In this paper $\mathrm{tr}(\cdot)$ denotes the matrix trace operator, $\mathrm{diag}(\cdot)$ denotes the diagonal matrix, $\lambda_{\min}(\cdot)$ ($\lambda_{\max}(\cdot)$) the minimum (maximum) eigenvalue, $\|\cdot\|_2$ denotes the Euclidean norm, and $\|\cdot\|_F$ denotes Frobenius matrix norm. Furthermore, $\mathrm{Var}(x)$ denotes the variance of vector x, and $\mathrm{MaxDev}(\cdot)$ denotes the maximum deviation of vector x from its normal value.

2.2. System description

The power circuit and the control diagram of a DC microgrid focusing on the structure of a DGU is shown in Fig. 2, where $I_{Li}(t)$, $I_i(t)$, and $V_i(t)$, denote the load current, the output current, and the load voltage, respectively, and C_{ti}, L_{ti}, R_{ti}, R_{ij} are the filter capacitor, filter inductance, filter resistance, and line resistance, respectively. The sensors measure V_{ds}, $V_i(t)$, $I_i(t)$, and $I_{Li}(t)$. As shown in this figure, the control structure consists of three parts of (i)- secondary control, (ii)- primary control, and (iii)- gate drive and PWM [38,39], which are not more elaborated due to space limitation.

The dynamic equations of each DGU is represented as [40]:

$$\frac{\mathrm{d}V_i(t)}{\mathrm{d}t} = \frac{1}{C_{ti}}(I_i(t) - I_{Li}(t)) + \sum_{j\in\mathcal{N}_i} \frac{1}{C_{ti}R_{ij}}(V_j(t) - V_i(t)),$$
$$\frac{\mathrm{d}I_i(t)}{\mathrm{d}t} = -\frac{1}{L_{ti}}V_i(t) - \frac{R_{ti}}{L_{ti}}I_i(t) + \frac{1}{L_{ti}}V_{ti}(t),\ i = 1,\dots,N, \tag{1}$$

where, $I_i(t)$ and $V_i(t)$ are states of the system, and $I_{Li}(t)$ and $V_{ti}(t)$ are inputs of the system. Furthermore, $V_j(t)$ is the output voltage of the neighboring jth DGU, $\mathcal{N}_i$ is the set of neighboring DGUs of the ith DGU with directly connected power line, and the resistance of the power line that connects the ith DGU to the jth DGU is denoted by R_{ij}.

Eq. (1) can be written in the state space representation as

$$\dot{x}_i(t) = A_{ii}x_i(t) + \sum_{j\in\mathcal{N}_i} A_{ij}x_j(t) + B_i u_i^c(t) + E_i d_i'(t), \tag{2}$$

where $x_i(t)$, $u_i^c(t)$, and $d_i'(t)$ denote the local state, the control input, and the exogenous/disturbance input, respectively and defined as $x_i(t) \triangleq [V_i(t), I_i(t)]^{\mathrm{T}}$, $u_i^c(t) \triangleq V_{ti}(t)$, and $d_i'(t) = I_{Li}(t)$. A_{ii} and A_{ij} denote the local state transition matrix, and the interconnection between subsystems i and j, respectively. Furthermore, B_i and E_i denote the primary and secondary transition matrices, respectively. These matrices are defined as follows [40]:

$$A_{ii} = \begin{bmatrix} \sum_{j\in\mathcal{N}_i} -\frac{1}{R_{ij}C_{ti}} & \frac{1}{C_{ti}} \\ -\frac{1}{L_{ti}} & -\frac{R_{ti}}{L_{ti}} \end{bmatrix}, A_{ij} = \begin{bmatrix} \frac{1}{R_{ij}C_{ti}} & 0 \\ 0 & 0 \end{bmatrix},$$
$$B_i = \begin{bmatrix} 0 \\ \frac{1}{L_{ti}} \end{bmatrix}, E_i = \begin{bmatrix} -\frac{1}{C_{ti}} \\ 0 \end{bmatrix},$$

The following primary controller, a decentralized state feedback controller with integral action, is considered to regulate the voltage at each DGU and guarantee the stability of the overall microgrid [40]:

$$\dot{\zeta}_i(t) = V_{\mathrm{ref},i}(t) - V_i(t) + \alpha_i(t),$$
$$u_i^c(t) = K_{i1}x_i(t) + K_{i2}\zeta_i(t), \tag{3}$$

where $\zeta_i(t)$ is the integrator state, $V_{\mathrm{ref},i}(t)$ is the voltage reference, $K_{i1} \in \mathbb{R}^{1\times 2}$ and $K_{i2} \in \mathbb{R}$ are constant primary controller gains. The consensus protocol based secondary control $\alpha_i(t) \in \mathbb{R}$ for achieving proportional current sharing is defined as [41]:

$$\dot{\alpha}_i(t) = -k_{\mathrm{I},i} \sum_{j\in\mathcal{N}_i} a_{ij}\left(\frac{I_i(t)}{I_i^s} - \frac{I_j(t)}{I_j^s}\right), \tag{4}$$

where $k_{\mathrm{I},i}$ is a constant to be designed, and I_i^s is constant scaling factor proportional to the DGU generation capacity. Fig. 2 shows this control structure.

It is assumed that the closed-loop microgrid has the desired performance with primary and secondary controllers given by (3) and (4).

Remark 1. It should be noted that the proposed FTC approach is independent of the primary and secondary controllers and any other hierarchical controller approach can be used.

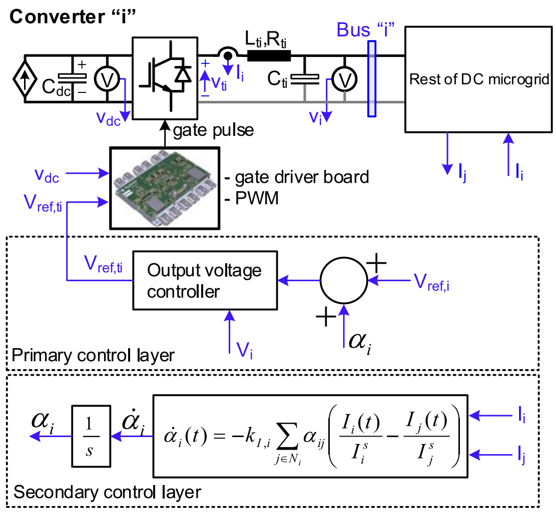

Fig. 2. A control structure and power circuit diagram of a DGU in a DC-microgrid.

2.3. Fault description

Different type of faults are introduced in Section 1. This paper focuses on the non-severe faults of Category D, which classifies the faults occurring from $V_{\mathrm{ref},ti}$ to V_{ti} in Fig. 2. In practice, such faults include "errors/mismatches in the DC-link voltage sensor", "errors/problems in analog circuits", "mis-operation of driver board", "errors/aging in switching elements", and etc.

From FTC design perspective, the most general form of fault modeling is achieved by using multiplicative and additive time-varying components. In that sense, the following equation is utilized in this paper for modeling of non-severe faults of Category D in Section 1.

$$V_{ti}(t) = \theta_i(t)\big(V_{\mathrm{ref},ti}(t) + f_i(t)\big), \tag{5}$$

where, $\theta_i(t)$ representing the multiplicative part of fault, is unknown time-varying scalar such that $0 < \theta_{i,\min} \le \theta_i(t) \le 1$ and $|\dot{\theta}_i(t)| \le \dot{\theta}_{i,\max}$, where $\theta_{i,\min}$ and $\dot{\theta}_{i,\max}$, are known positive scalars. Furthermore, $f_i(t)$ is the time-varying additive part of fault in the ith DGU which occurs at $t_i^{\mathrm{f}} > 0$, where $f_i(t) = 0$, for $t < t_i^{\mathrm{f}}$, and $|f_i(t)| \le f_{i,\max}$, and $|\dot{f}_i(t)| \le \dot{f}_{i,\max}$, with known constants $f_{i,\max}$ and $\dot{f}_{i,\max}$.

2.4. Problem formulation

Based on (2) and (5), the dynamics of the ith faulty DGU is formulated as follows

$$\dot{x}_i^{\mathrm{f}}(t) = A_{ii}x_i^{\mathrm{f}}(t) + \sum_{j\in\mathcal{N}_i} A_{ij}x_j^{\mathrm{f}}(t) + B_i^{\mathrm{f}}(t)\big(u_i^{\mathrm{f}}(t) + f_i(t)\big) + E_i d_i'(t), \quad i = 1,2,\dots,N, \tag{6}$$

where $x_i^{\mathrm{f}}(t), x_j^{\mathrm{f}}(t) \in \mathbb{R}^2$ denote the state of the ith and jth DGUs in the presence of fault, $u_i^{\mathrm{f}}(t) \in \mathbb{R}$ is the output of the ith DGU adaptive FTC module, and $B_i^{\mathrm{f}}(t) = B_i\theta_i(t)$. As shown in (6), additive faults and disturbances have a similar role in the system's performance from a modeling perspective. However, multiplicative faults have a different role and may even lead to instability. It is worth noting that disturbances have no effect on the stability of the system, while faults, especially multiplicative faults, can lead to instability.

In our approach, an adaptive FTC module based on the idea of fault-hiding approach [42–44], is located between the faulty DGU and the nominal primary controller to hide the faults from the nominal primary controller after its occurrence. $u_i^{\mathrm{c}}(t)$ and $x_i^{\mathrm{f}}(t)$ are inputs of the FTC module and $\tilde{x}_i(t)$ and $u_i^{\mathrm{f}}(t)$ are its outputs.

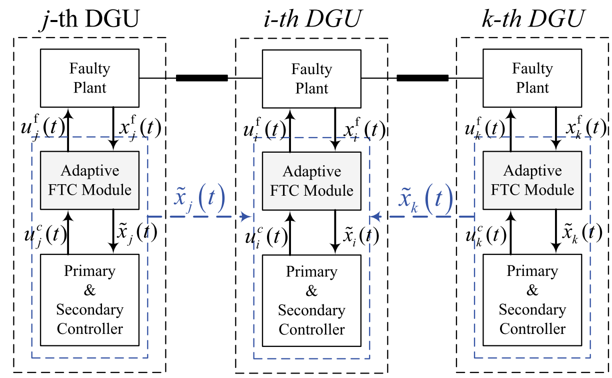

Fig. 3. The physical and communication connection of the ith DGU microgrid with its neighbors (the jth and kth DGUs).

The reference model of healthy DGU used in the proposed FTC module is:

$$\dot{\tilde{x}}_i(t) = A_{ii}\tilde{x}_i(t) + \sum_{j\in\mathcal{N}_i} A_{ij}\tilde{x}_j(t) + B_i u_i^{\mathrm{c}}(t) + E_i d_i'(t), \tag{7}$$

where $\tilde{x}_i(t) \in \mathbb{R}^2$ denotes the reference model state. Based on Fig. 3, the ith DGU, $i = 1,\dots,N$, receives states of the reference model of neighbors ($\tilde{x}_j(t)$, $j \in \mathcal{N}_i$) instead of their actual states in the proposed FTC, and they are used in the primary/secondary controller and the FTC module of the ith DGU to construct $u_i^{\mathrm{c}}(t)$ and $u_i^{\mathrm{f}}(t)$. The state $\tilde{x}_i(t)$ is bounded and has the desired behavior, since $\tilde{x}_i(t)$, $i = 1,\dots,N$, is the state of ith healthy DGU.

The recovery error signal for each DGU is defined as

$$x_i^{\Delta}(t) \triangleq x_i^{\mathrm{f}}(t) - \tilde{x}_i(t). \tag{8}$$

Based on this definition, $x_i^{\mathrm{f}}(t)$ is bounded if $x_i^{\Delta}(t)$ and $x_j^{\Delta}(t)$, $j \in \mathcal{N}_i$, is bounded.

Definition 1. The faulty microgrid fully recovers its performance, if

$$\lim_{t\to\infty} x^{\Delta}(t) = 0, \tag{9}$$

where

$$x^{\Delta}(t) \triangleq \left[x_1^{\Delta^{\mathrm{T}}}(t), x_2^{\Delta^{\mathrm{T}}}(t), \dots, x_N^{\Delta^{\mathrm{T}}}(t)\right]^{\mathrm{T}}. \tag{10}$$

In this paper, an adaptive FTC module is designed to recover the performance of microgrid after the occurrence faults.

3. Adaptive FTC design

In order to design an adaptive FTC module, we need to represent the dynamics of the reference model given by (7) in the controller canonical representation as:

$$\dot{\hat{x}}_i(t) = \hat{A}_{ii}\hat{x}_i(t) + \sum_{j\in\mathcal{N}_i} \hat{A}_{ij}\hat{x}_j(t) + \hat{B}_i u_i^{\mathrm{c}}(t) + \hat{E}_i d_i'(t), \tag{11}$$

where $\hat{x}_i(t) \triangleq T_i\tilde{x}_i(t)$, $\hat{x}_j \triangleq T_i\tilde{x}_j$, and $T_i \triangleq \left[q_i^{\mathrm{T}}, (q_i A_{ii})^{\mathrm{T}}\right]^{\mathrm{T}}$, where q_i is the last row of $C_c^{i^{-1}} \triangleq \left[B_i, A_{ii}B_i\right]^{-1}$. Furthermore, $\hat{A}_{ij} \triangleq T_i A_{ij} T_i^{-1}$, $\hat{E}_i = T_i E_i$,

$$\hat{A}_{ii} \triangleq T_i A_{ii} T_i^{-1} = \begin{bmatrix} 0 & 1 \\ -d_0^i & -d_1^i \end{bmatrix}, \tag{12}$$

$$\hat{B}_i \triangleq \begin{bmatrix} 0 & 1 \end{bmatrix}^{\mathrm{T}}, \tag{13}$$

with d_0^i and d_1^i are scalars. Similarly, the dynamics given by (6) can be represented as

$$\dot{\hat{x}}_i^{\mathrm{f}}(t) = \hat{A}_{ii}\hat{x}_i^{\mathrm{f}}(t) + \sum_{j\in\mathcal{N}_i} \hat{A}_{ij}\hat{x}_j^{\mathrm{f}}(t) + \hat{B}_i^{\mathrm{f}}(t)\big(u_i^{\mathrm{f}}(t) + f_i(t)\big) + \hat{E}_i d_i'(t), \quad \hat{x}_i^{\mathrm{f}}(0) = \hat{x}_{i0}^{\mathrm{f}}, \quad i = 1,2,\dots,N, \tag{14}$$

where $\hat{x}_i^{\mathrm{f}}(t) \triangleq T_i x_i^{\mathrm{f}}(t)$, $\hat{x}_j^{\mathrm{f}}(t) \triangleq T_i x_j^{\mathrm{f}}(t)$, $\hat{x}_{i0}^{\mathrm{f}} \triangleq T_i x_{i0}^{\mathrm{f}}$ and $\hat{B}_i^{\mathrm{f}}(t) \triangleq T_i B_i^{\mathrm{f}}(t)$.

Theorem 1. *Consider the dynamics of closed-loop system described by (3), (4) and (6) with the FTC module output:*

$$u_i^{\mathrm{f}}(t) = M_i(t)x_i^{\Delta}(t) + n_i(t)u_i^{\mathrm{c}}(t) - \hat{f}_i(t), \tag{15}$$

and update laws

$$\dot{M}_i(t) = \mathrm{Proj}_{\mathrm{m}}\left[M_i(t), -B_i^{\mathrm{T}}P_i x_i^{\Delta}(t) x_i^{\Delta^{\mathrm{T}}}(t)\right]\Gamma_{\mathrm{M}_i}, \tag{16}$$

$$\dot{n}_i(t) = \gamma_{\mathrm{n}_i}\mathrm{Proj}\left[n_i(t), -B_i^{\mathrm{T}}P_i x_i^{\Delta}(t)u_i^{\mathrm{c}}(t)\right], \tag{17}$$

$$\dot{\hat{f}}_i(t) = \gamma_{\mathrm{f}_i}\mathrm{Proj}\left[\hat{f}_i(t), B_i^{\mathrm{T}}P_i x_i^{\Delta}(t)\right], \tag{18}$$

with $M_i(0) = M_{i0}$, $n_i(0) = n_{0i}$, $\hat{f}_i(0) = \hat{f}_{i0}$, $\Gamma_{\mathrm{M}_i} \in \mathbb{R}^{2\times 2}$ is positive definite gain matrix, γ_{n_i} and γ_{f_i} are positive constants, $P_i \triangleq T_i^{\mathrm{T}}\hat{P}_i T_i$. Then, there exist bounded scalars $\mathcal{T}$, $\tilde{M}_{i,\max}$, $\tilde{f}_{i,\max}$, $\tilde{n}_{i,\max}$, $\underline{n}^*_{i,\max}$, $\dot{\underline{n}}^*_{i,\max}$, $\dot{n}^*_{i,\max}$, $\dot{f}_{i,\max}$, and $\dot{M}^*_{i,\max}$, $i = 1, 2, \ldots, N$, such that $x^{\Delta}(t)$ is bounded with ultimate bound $\|x^{\Delta}(t)\|_2 < \epsilon$, $t \geq \mathcal{T}$, where

$$\epsilon = \left[\frac{\|T^{-1}\|_2^2}{\lambda_{\min}(\hat{P})}\left(\lambda_{\max}(\hat{P})\nu^2 + \sum_{i\in N}\underline{n}^*_{i,\max}\left[\lambda_{\max}(\Gamma_{\mathrm{M}_i}^{-1})\tilde{M}_{i,\max}^2 + \gamma_{\mathrm{n}_i}^{-1}\tilde{n}_{\max}^2 + \gamma_{\mathrm{f}_i}^{-1}\tilde{f}_{i,\max}^2\right]\right)\right]^{\frac{1}{2}}, \tag{19}$$

$$\nu \triangleq \left[\frac{1}{\lambda_{\min}(Q)}\sum_{i\in N}\left[\dot{\underline{n}}^*_{i,\max}\left(\gamma_{\mathrm{n}_i}^{-1}\tilde{n}_{i,\max}^2 + \lambda_{\max}(\Gamma_{\mathrm{M}_i}^{-1})\tilde{M}_{i,\max}^2 + \gamma_{\mathrm{f}_i}^{-1}\tilde{f}_{i,\max}^2\right) + \underline{n}^*_{i,\max}\left(2\gamma_{\mathrm{n}_i}^{-1}\tilde{n}_{i,\max}\dot{n}^*_{i,\max} + 2\lambda_{\max}(\Gamma_{\mathrm{M}_i}^{-1})\tilde{M}_{i,\max}\dot{M}^*_{i,\max} + 2\gamma_{\mathrm{f}_i}^{-1}\tilde{f}_{i,\max}\dot{f}_{i,\max}\right)\right]\right]^{\frac{1}{2}}$$

if there exist matrices $A_i^{\mathrm{d}} \in \mathbb{R}^{2\times 2}$, $i = 1, \ldots, N$, with the similar structure given in (12) and positive definite matrices $\hat{P}_i \in \mathbb{R}^{2\times 2}$, $i = 1, \ldots, N$, such that

$$-Q \triangleq \begin{bmatrix} Q_{11} & Q_{12} + Q_{21}^{\mathrm{T}} & \cdots & Q_{1N} + Q_{N1}^{\mathrm{T}} \\ Q_{21} + Q_{12}^{\mathrm{T}} & Q_{22} & \cdots & Q_{2N} + Q_{N2}^{\mathrm{T}} \\ \vdots & \vdots & \ddots & \vdots \\ Q_{N1} + Q_{N1}^{\mathrm{T}} & Q_{N2} + Q_{2N}^{\mathrm{T}} & \cdots & Q_{NN} \end{bmatrix} < 0, \tag{20}$$

where $T \triangleq \mathrm{diag}(T_1, \ldots, T_N)$, $\hat{P} \triangleq \mathrm{diag}(\hat{P}_1, \ldots, \hat{P}_N)$ and

$$Q_{ii} \triangleq \hat{P}_i A_i^{\mathrm{d}} + A_i^{\mathrm{d}^{\mathrm{T}}}\hat{P}_i, \qquad i = 1, \ldots, N$$

$$Q_{ij} \triangleq \begin{cases} \hat{P}_i\hat{A}_{ij}, & j \in \mathcal{N}_i, \\ 0, & j \notin \mathcal{N}_i, \end{cases} \qquad i, j = 1, \ldots, N$$

Moreover, for constant additive and loss of effectiveness faults, the performance of the microgrid is fully recovered ($x_i^{\Delta}(t)$ tends to zero).

Proof. See Appendix B.

As can be seen from (15) to (18), the parameters of compensator is independent from the parameters of the primary and secondary controllers. Therefore, changing the primary and secondary controllers do not affect the parameters of compensator. This feature is one of the main key factors of the proposed approach.

Next proposition shows how one can solve the matrix inequality given by (20).

Proposition 1. *The matrix inequality given by (20) with setting $\hat{P}_i = \bar{P}$, $i = 1, \ldots, N$, is satisfied for A_i^{d} with the similar structure given in (12) and a positive definite matrix $\bar{P} \in \mathbb{R}^{2\times 2}$ if and only if there exist vectors $W_i \in \mathbb{R}^2$, $i = 1, \ldots, N$, and a positive definite matrix $Z \in \mathbb{R}^{2\times 2}$, such that the following LMI is satisfied:*

$$\begin{bmatrix} \Xi_{11} & \Xi_{12} + \Xi_{21}^{\mathrm{T}} & \Xi_{13} + \Xi_{31}^{\mathrm{T}} & \cdots & \Xi_{1N} + \Xi_{N1}^{\mathrm{T}} \\ * & \Xi_{22} & \Xi_{23} + \Xi_{32}^{\mathrm{T}} & \cdots & \Xi_{2N} + \Xi_{N2}^{\mathrm{T}} \\ * & * & \Xi_{33} & \cdots & \Xi_{3N} + \Xi_{N3}^{\mathrm{T}} \\ \vdots & \vdots & \vdots & \ddots & \vdots \\ * & * & * & \cdots & \Xi_{NN} \end{bmatrix} < 0, \tag{21}$$

where $Z \triangleq \bar{P}^{-1}$, $\Xi_{ii} \triangleq A_0 Z + Z A_0^{\mathrm{T}} - B_0 W_i^{\mathrm{T}} - W_i B_0^{\mathrm{T}}$, $i = 1, \ldots, N$,

$$\Xi_{ij} \triangleq \begin{cases} \hat{A}_{ij}Z, & j \in \mathcal{N}_i, \\ 0, & j \notin \mathcal{N}_i, \end{cases} \qquad i, j = 1, \ldots, N,$$

and

$$A_0 \triangleq \begin{bmatrix} 0 & 1 \\ 0 & 0 \end{bmatrix}, \quad B_0 \triangleq \begin{bmatrix} 0 \\ 1 \end{bmatrix}. \tag{22}$$

Proof. See Appendix C.

Remark 2. Γ_{M_i}, Γ_{N_i} and γ_{f_i} are design parameters and they are chosen based on the desired performance of the system and by trial and error. One can make the ultimate bound given in (19) arbitrarily small if $\lambda_{\min}(\Gamma_{\mathrm{M}_i})$, $\lambda_{\min}(\Gamma_{\mathrm{N}_i})$ and γ_{f_i} are large enough. It should be noted that the very large value selection of these parameters causes the large value of the control input and even some computational issues.

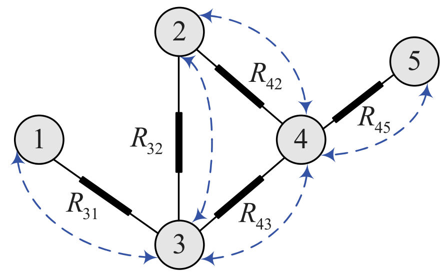

Fig. 4. Interconnection of 5 DGUs in a DC microgrid network.

Table 2
The output filter values of DGUs.

DGU	Capacitance C_t (mF)	Resistance R_t (Ω)	Inductance L_t (mH)
DGU 1	2.2	0.2	1.8
DGU 2	1.9	0.3	2.0
DGU 3	1.7	0.1	2.2
DGU 4	2.5	0.5	3.0
DGU 5	2.0	0.4	1.3

Table 3
The interconnecting line parameters.

Connected DGUs	Inductance L_{ij} (μH)	Resistance R_{ij} (Ω)
(1,3)	2.1	0.07
(2,3)	2.3	0.04
(2,4)	1.8	0.08
(3,4)	1	0.07
(4,5)	2	0.05

4. Simulation results

Fig. 4 shows the studied multi-converter DC microgrid test system with a complex mesh structure. To control the DGUs, a consensus-based secondary controller is used in this paper, which contains a undirected communication graph represented by dashed lines. The implemented primary and secondary controllers are given by (3) and (4) with controller gains obtained from [45]. The output filter values and the interconnecting lines parameters of DGUs are shown in Tables 2 and 3, respectively. The nominal operating point voltage and current values of DGUs are $\bar{V}_{\mathrm{ref}} = [40, 50, 48, 42, 46]^{\mathrm{T}}$ V and $\bar{I}_{\mathrm{ref}} = [20, 80, 40, 80, 20]^{\mathrm{T}}$ A, respectively.

To design the proposed FTC modules of (15)–(18), the matrix P_i is obtained according to Proposition 1. Design parameters are set at $\Gamma_{\mathrm{M}_i} = 100000 I_2$, $\gamma_{\mathrm{n}_i} = 50000$, and $\gamma_{\mathrm{f}_i} = 5000$, $i = 1, \ldots, 5$.

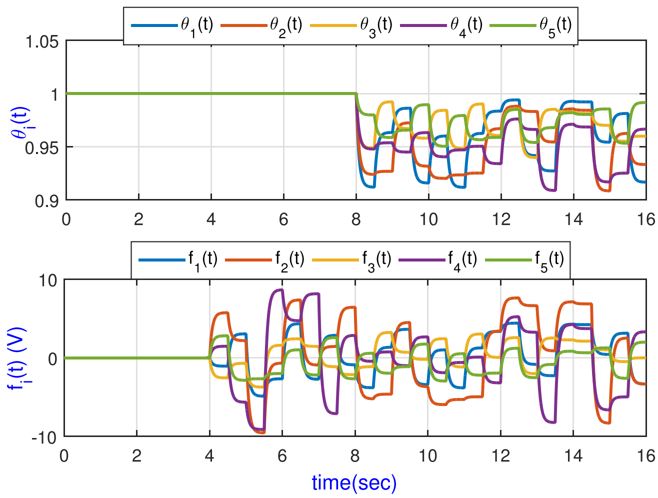

Fig. 5. The multiplicative and additive component of considered fault condition of category-E with random variation, (top) multiplicative component of $\theta_i(t)$, (bottom) additive component of $f_i(t)$.

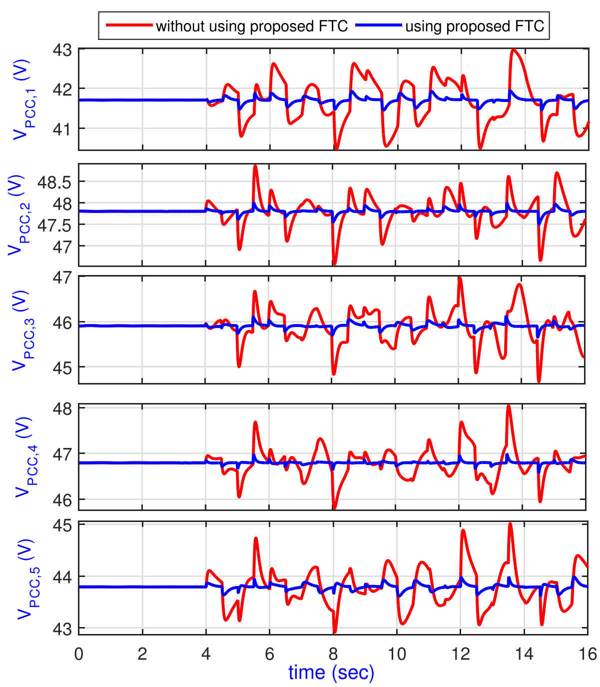

Fig. 6. The output voltages of DGUs under non-severe fault condition of Category E with/without using the proposed FTC.

4.1. Case study 1: Fault condition scenarios

To apply the non-severe fault condition of Category D, the general fault format of (5) is applied to the terminal voltage references generated by the controller. Fig. 5 shows the parameters of the applied faults $\theta_i(t)$ and $f_i(t)$, $i = 1, \ldots, 5$, generated by random function to show the random and unknown nature of the studied faults. The additive $f_i(t)$ and the multiplicative $\theta_i(t)$ parts of the fault are applied at $t = 4.0$ sec. and $t = 8.0$ sec., respectively. The amplitude of the fault parameters are chosen such that the resulted faults do not saturate/disable the controllers, otherwise the fault is severe fault, and the protection system should be activated. The studied condition is the worst possible case of non-severe fault of Category D.

Table 4
Statistical parameters of the performance of DGUs without using the proposed method.

	DGU1	DGU2	DGU3	DGU4	DGU5	Max. value
Var($V_i(t)$) in [V]	0.24	0.09	0.10	0.08	0.11	0.24
MaxDev($V_i(t)$) in [V]	1.3	1.1	1	1.2	1.3	1.3
Var($I_i(t)$) in [A]	19	79	129	75	22	129
MaxDev($V_i(t)$) in [A]	13	29	41	24	10	41

Table 5
Statistical parameters of the performance of DGUs with using the proposed method.

	DGU1	DGU2	DGU3	DGU4	DGU5	Max. value
Var($V_i(t)$) in [V]	0.0051	0.0022	0.0020	0.0007	0.0026	0.0051
MaxDev($V_i(t)$) in [V]	0.24	0.30	0.22	0.20	0.28	0.28
Var($I_i(t)$) in [A]	0.34	1.40	1.57	0.94	0.75	1.57
MaxDev($I_i(t)$) in [A]	1.53	4.32	4.36	3.26	2.64	4.36

The output voltages and currents of DGUs are depicted in Figs. 6 and 7, respectively. In these figures, the conventional controllers of the DGUs are implemented with/without proposed FTC scheme. As shown in the figures, the deviation of the voltage waveforms from nominal values is negligible using the proposed FTC method. Also, the deviation is at most 2.5% for the cases without using the proposed FTC, which is still acceptable. Statistical parameters of the performance of DGUs without and with using the proposed method such as the variance of the voltage and the current as well as their maximum deviation from their normal values are shown in Tables 4 and 5. These results show that the considered fault is non-severe and the DC-microgrid is still stable while using the proposed FTC approach, the voltage and current deviations of DGU are significantly reduced. To more explain the results, Fig. 7 clearly reveals the impact of the faults. As shown in this figure, the current sharing among the DGUs is considerably affected by the faults, which even causes 100% deviation and oscillation in the output current of DGUs. As shown in the figure, the output current of DGU3 even approaches to zero in some instants. The results show the worst possible case of non-severe fault of Category D, in which although the DC-microgrid is stable, the current sharing is considerably destroyed by occurrence of the faults. Using the proposed FTC scheme, the results show that the current sharing is still very close to normal condition, showing the effectiveness of the proposed scheme.

4.2. Case study 2: Impact of system parameter variation

Generally, the nominal values of the electrical quantities are used in designing FTC schemes, as can be seen in (7) and (15)–(18). However, the parameters may change by time and under different operating conditions, and also, they have some uncertainties in their values. This sub-section provides a scenario to investigate the performance of the proposed FTC under parameters value changes. In this scenario, the resistance R_{23} and the inductance L_{t3} are reduced by 20% from their nominal values. It is worth noting that the proposed FTC is designed based on the nominal values of the parameters. The fault conditions of the previous sub-section is applied to the studied system, and the results are given in the following. Figs. 8 and 9 show the voltage and current waveforms for three cases of (i) the conventional system without using the proposed FTC, (ii) the conventional system using the proposed FTC without any uncertainties in the parameters (FTC-E), and (iii) the conventional system using the proposed FTC in the presence of 20% uncertainty in the values of R_{23} and L_{t3} (FTC-N). Furthermore, Table 6 shows the statistical parameters of the performance of DGUs in this scenario. As depicted in these figures and this table, the output of the proposed FTC with uncertainties is very similar to that of without uncertainty. This result shows that using the proposed scheme, the performance of DGUs is not seriously affected by the changes in the model parameters and uncertainty in the parameter values.

Table 6
Statistical parameters of the performance of DGUs with using the proposed method in case of uncertainties in the nominal values of electrical parameters.

	DGU1	DGU2	DGU3	DGU4	DGU5	Max. value
Var($V_i(t)$) in [V]	0.0051	0.0022	0.0020	0.0007	0.0026	0.0051
MaxDev($V_i(t)$) in [V]	0.24	0.29	0.23	0.20	0.28	0.28
Var($I_i(t)$) in [A]	0.33	1.45	1.62	0.94	0.75	1.62
MaxDev($I_i(t)$) in [A]	1.4	6.3	2.56	3.19	2.63	6.3

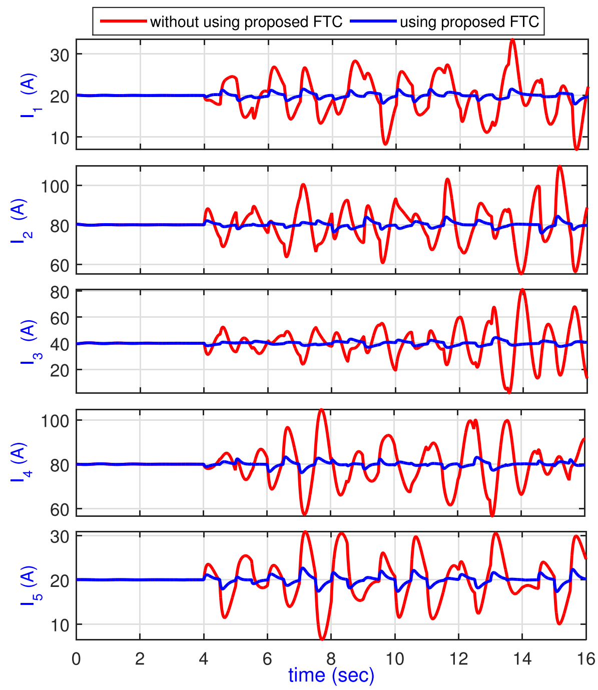

Fig. 7. The output currents of DGUs (current sharing) under non-severe fault condition of Category E with/without using the proposed FTC.

5. Conclusion

This paper proposes an adaptive voltage compensator scheme for converters in a multi-converter DC-microgrids (MGs). The proposed scheme compensates the impact of the faults, and the controllers of the distributed generation units (DGUs) can operate similar to the normal operation with proper performance using the proposed compensator. Due to the complex and unknown behavior of the faults, the faults are modeled by random time-varying multiplicative and additive components, which inherently considers the most general case of fault condition. To verify the effectiveness of the proposed scheme, various fault condition scenarios are analyzed in a multi-converter DC microgrid test system with a complex mesh structure. With refer to the results, under the considered worst possible fault condition, the current sharing among the DGUs is lost without using FTC method. In such cases, considerable oscillation occurs on the output current of the DGUs, which reduces the output current of some DGUs and overloads some others by even 100%. Using the proposed voltage control scheme, the current sharing is very close to the normal operating condition of the system. Also, to show the robustness against DC-microgrid parameters change, a fault condition scenario with 20% uncertainty is considered. The results shows that the proposed approach properly operate under conditions with uncertainty in the parameter values.

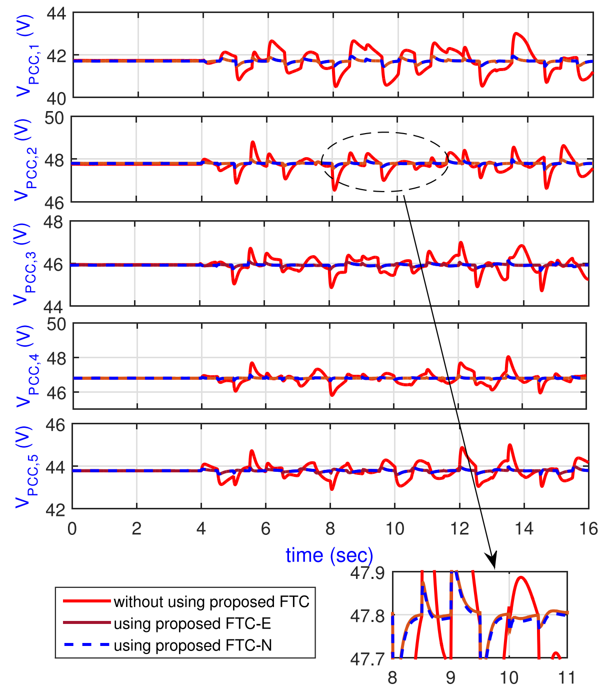

Fig. 8. The output voltages of DGUs under non-severe fault condition of Category E with three different situations, (1) without using the proposed FTC and without any uncertainty in the parameters, (2) using the proposed FTC without any uncertainty in the parameters (FTC-E), and (3) using the proposed FTC with 20% uncertainties in the parameters of the DC-microgrid (FTC-N).

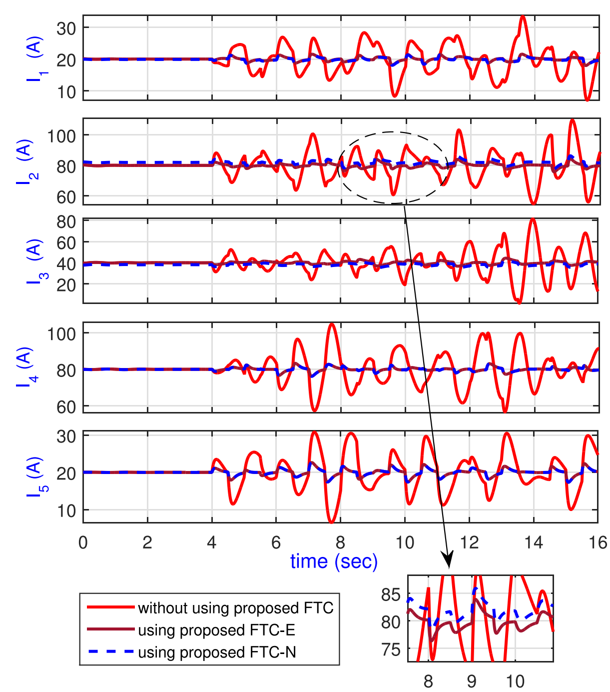

Fig. 9. The output currents of DGUs (current sharing) under non-severe fault condition of Category E with three different situations, (1) without using the proposed FTC and without any uncertainty in the parameters, (2) using the proposed FTC without any uncertainty in the parameters (FTC-E), and (3) using the proposed FTC with 20% uncertainties in the parameters of the DC-microgrid (FTC-N).

CRediT authorship contribution statement

Meysam Yadegar: Methodology, Investigation, Software, Validation, Data curation, Writing – original draft, Conceptualization, Writing – review & editing. **Seyed Fariborz Zarei:** Investigation, Validation, Data curation, Writing – original draft, Conceptualization, Writing – review & editing. **Nader Meskin:** Writing – review & editing, Conceptualization, Supervision. **Ahmed Massoud:** Writing – review & editing.

Declaration of competing interest

All authors declare that there are no known conflicts of interest associated with this publication and there has been no significant financial support for this work that could have influenced its outcome.

Data availability

No data was used for the research described in the article.

Appendix A. Preliminaries

Definition 2 (*[46]*). If $\phi : \mathbb{R}^n \longrightarrow \mathbb{R}$ is a continuously differentiable convex function with $\phi(\theta) \triangleq \frac{(\epsilon_\theta+1)\theta^{\mathrm{T}}\theta-\theta_{\max}^2}{\epsilon_\theta\theta_{\max}^2}$ where $\theta_{\max} \in \mathbb{R}$ is a *projection norm bound* imposed on $\theta \in \mathbb{R}^n$, and $\epsilon_\theta > 0$ is a*projection tolerance bound*, then, the *projection operator* $\mathrm{Proj} : \mathbb{R}^n \times \mathbb{R}^n \longrightarrow \mathbb{R}^n$ is defined by

$$\mathrm{Proj}(\theta, y) \triangleq \begin{cases} y, & \text{if } \phi(\theta) < 0, \\ y, & \text{if } \phi(\theta) \geq 0 \text{ and } \phi'(\theta)y \leq 0, \\ y - \frac{\phi'^{\mathrm{T}}(\theta)\phi'(\theta)y}{\phi'(\theta)\phi'^{\mathrm{T}}(\theta)}\phi(\theta), & \text{if } \phi(\theta) \geq 0 \text{ and } \phi'(\theta)y > 0, \end{cases}$$

where $y \in \mathbb{R}^n$ and $\phi'(\theta) \triangleq \dfrac{\partial\phi(\theta)}{\partial\theta}$.

It can be shown that the solution of $\dot{\theta}(t) = \mathrm{Proj}(\theta(t), y(t))$ remains in $\Omega_1 \triangleq \{\theta \in \mathbb{R}^n : \phi(\theta) \leq 1\} = \{\theta \in \mathbb{R}^n : |\theta| \leq \theta_{\max}\}$, for every $y(t)$, $t \geq 0$, and $\theta(0) \in \Omega_0 \triangleq \{\theta \in \mathbb{R}^n : \phi(\theta) \leq 0\} = \{\theta \in \mathbb{R}^n : |\theta| \leq \frac{\theta_{\max}}{\sqrt{1+\epsilon_\theta}}\}$. For details, see [47,48]. It follows from Definition 2 that [48]

$$(\theta - \theta^*)^{\mathrm{T}}(\mathrm{Proj}(\theta, y) - y) \leq 0, \;\; \theta^* \in \mathbb{R}^n, \;\; \phi(\theta^*) < 0. \tag{A.1}$$

The definition of the projection operator is generalized to matrices as $\mathrm{Proj}_{\mathrm{m}} = \big(\ \mathrm{Proj}(\mathrm{col}_1(\Theta), \mathrm{col}_1(Y)), \ldots, \mathrm{Proj}(\mathrm{col}_m\ (\Theta), \mathrm{col}_m(Y))\ \big)$, where $\Theta \in \mathbb{R}^{n\times m}$, $Y \in \mathbb{R}^{n\times m}$ and $\mathrm{col}_i(\cdot)$ denotes the ith column operator. In this case, for a given $\Theta^* \in \mathbb{R}^{n\times m}$, it follows from (A.1) that [49]

$$\begin{aligned} &\mathrm{tr}\left[(\Theta - \Theta^*)^{\mathrm{T}}(\mathrm{Proj}_{\mathrm{m}}(\Theta, Y) - Y)\right] \\ &= \sum_{i=1}^{m}\left[\mathrm{col}_i(\Theta - \Theta^*)^{\mathrm{T}}\big(\mathrm{Proj}(\mathrm{col}_i(\Theta), \mathrm{col}_i(Y)) - \mathrm{col}_i(Y)\big)\right] \leq 0. \end{aligned} \tag{A.2}$$

The following lemmas are needed in the paper.

Lemma 1 (*[50]*). *Let $P \in \mathbb{R}^{n\times n}$ be a symmetric matrix and $Q \in \mathbb{R}^{n\times n}$ be a nonnegative-definite matrix. Then $\lambda_{\min}(P)\mathrm{tr}(Q) \leq \mathrm{tr}(PQ) \leq \lambda_{\max}(P)\mathrm{tr}(QB)$.*

Appendix B. Proof of Theorem 1

Proof. First consider the following proposition:

Proposition 2. *There exist $M_i^*(t) \in \mathbb{R}^{1\times 2}$, $n_i^*(t) \in \mathbb{R}^+$, and positive constants $M_{i,\max}$ $\dot{M}_{i,\max}$, $\underline{n}_{i,\min}^*$, and $\underline{\dot{n}}_{i,\max}^*$, $i = 1, \ldots, N$, such that*

$$\begin{cases} \hat{B}_i^{\mathrm{f}}(t)n_i^*(t) - \hat{B}_i = 0, \\ \underline{n}_{i,\min}^* \leq n_i^{*-1}(t) \leq 1, \\ |\dot{n}_i^{*-1}(t)| \leq \underline{\dot{n}}_{i,\max}^*, \end{cases} \tag{B.1}$$

$$\begin{cases} \hat{A}_{ii} + \hat{B}_i^{\mathrm{f}}(t)M_i^*(t)T_i^{-1} = A_i^{\mathrm{d}}, \\ \|M_i^*(t)\|_{\mathrm{F}} \leq M_{i,\max}, \\ \|\dot{M}_i^*(t)\|_{\mathrm{F}} \leq \dot{M}_{i,\max}, \end{cases} \tag{B.2}$$

where A_i^{d} has similar structure given by (12) with positive scalars d_0^i and d_1^i and hence it is Hurwitz.

Proof. According to the structure of $B_i^{\mathrm{f}}(t)$, we can choose $n_i^*(t) = \theta_i^{-1}(t)$, and consequently, $\underline{n}_{i,\min}^* \triangleq \theta_{i,\min}$ and $\underline{\dot{n}}_{i,\max}^* \triangleq \dot{\theta}_{i,\max}$.

Based on the structure of $\hat{A}_{ii}$, $\hat{B}_i$, and A_i^{d}, there exists $K_i \in \mathbb{R}^{1\times 2}$ such that $\hat{A}_{ii} + \hat{B}_i K_i = A_i^{\mathrm{d}}$. Therefore

$$\hat{A}_{ii} + \hat{B}_i^{\mathrm{f}}(t)M_i^*(t)T_i^{-1} = A_i^{\mathrm{d}},$$

where $M_i^*(t) = \theta_i^{-1}(t)K_i T_i$. It is easy to show that $|\dot{\theta}_i^{-1}(t)| \leq \underline{\dot{\theta}}_{i,\max}$ with $\underline{\dot{\theta}}_{i,\max} \triangleq \dot{\theta}_{i,\max}/\theta_{i,\min}^2$. Therefore, it follows that: $M_{i,\max} \triangleq \|K_i\|_{\mathrm{F}}\|T_i\|_{\mathrm{F}}\frac{1}{\theta_{i,\min}}$ and $\dot{M}_{i,\max} \triangleq \|K_i\|_{\mathrm{F}}\|T_i\|_{\mathrm{F}}\underline{\dot{\theta}}_{i,\max}$ and this completes the proof. □

It follows from (11), (14) and (15) that

$$\begin{aligned} \dot{\hat{x}}_i^{\Delta}(t) =& \hat{A}_{ii}\hat{x}_i^{\Delta}(t) + \sum_{j\in\mathcal{N}_i}\hat{A}_{ij}\hat{x}_j^{\Delta}(t) + \hat{B}_i^{\mathrm{f}}(t)M_i(t)T_i^{-1}\hat{x}_i^{\Delta}(t) \\ &+ \hat{B}_i^{\mathrm{f}}(t)n_i(t)u_i^{\mathrm{c}}(t) + \hat{B}_i^{\mathrm{f}}(t)\big(f_i(t) - \hat{f}_i(t)\big) - \hat{B}_i u_i^{\mathrm{c}}(t) \\ =& \big(\hat{A}_{ii} + \hat{B}_i^{\mathrm{f}}(t)M_i^*(t)T_i^{-1}\big)\hat{x}_i^{\Delta}(t) + \sum_{j\in\mathcal{N}_i}\hat{A}_{ij}\hat{x}_j^{\Delta}(t) \\ &+ \hat{B}_i^{\mathrm{f}}(t)\tilde{M}_i(t)T_i^{-1}\hat{x}_i^{\Delta}(t) + \hat{B}_i^{\mathrm{f}}(t)\tilde{n}_i(t)u_i^{\mathrm{c}}(t) \\ &- \hat{B}_i^{\mathrm{f}}(t)\tilde{f}_i(t) + \big(\hat{B}_i^{\mathrm{f}}(t)n_i^*(t) - \hat{B}_i\big)u_i^{\mathrm{c}}(t), \end{aligned} \tag{B.3}$$

where $\tilde{n}_i(t) \triangleq n_i(t) - n_i^*(t)$, $\tilde{M}_i(t) \triangleq M_i(t) - M_i^*(t)$, and $\tilde{f}_i(t) \triangleq \hat{f}_i(t) - f_i(t)$.

$\|M_i(t)\|_{\mathrm{F}}$, $|n_i(t)|$, and $|f_i(t)|$ are bounded, since $M_i(t)$, $n_i(t)$, and $\hat{f}_i(t)$ are predicated on the projection operator. Hence, there exist positive constants $\tilde{f}_{i,\max}$, $\tilde{n}_{i,\max}$, and $\tilde{M}_{i,\max}$ such that $|\tilde{f}_i(t)| \leq \tilde{f}_{i,\max}$, $|\tilde{n}_i(t)| \leq \tilde{n}_{i,\max}$, and $\|\tilde{M}_i(t)\|_{\mathrm{F}} \leq \tilde{M}_{i,\max}$.

Eq. (B.3), using Proposition 1, can be written as

$$\begin{aligned} \dot{\hat{x}}_i^{\Delta}(t) =& A_i^{\mathrm{d}}\hat{x}_i^{\Delta}(t) + \sum_{j\in\mathcal{N}_i}\hat{A}_{ij}\hat{x}_j^{\Delta}(t) + \hat{B}_i^{\mathrm{f}}(t)\tilde{M}_i(t)T_i^{-1}\hat{x}_i^{\Delta}(t) \\ &+ \hat{B}_i^{\mathrm{f}}(t)\tilde{n}_i(t)u_i^{\mathrm{c}}(t) - \hat{B}_i^{\mathrm{f}}(t)\tilde{f}_i(t). \end{aligned} \tag{B.4}$$

We consider the Lyapunov candidate function as:

$$\begin{aligned} &V\big(\hat{x}^{\Delta}(t), \tilde{M}(t), \tilde{n}(t), \tilde{f}(t), t\big) \\ &\qquad = \sum_{i\in N} V_i\big(\hat{x}_i^{\Delta}(t), \tilde{M}_i(t), \tilde{n}_i(t), \tilde{f}_i(t), t\big) \end{aligned}$$

where $\tilde{n}(t) \triangleq [\tilde{n}_1(t), \ldots, \tilde{n}_N(t)]^{\mathrm{T}}$, $\tilde{f}(t) \triangleq [\tilde{f}_1(t), \ldots, \tilde{f}_N(t)]^{\mathrm{T}}$, $\tilde{M}(t) \triangleq \mathrm{diag}(\tilde{M}_1(t), \ldots, \tilde{M}_N(t))$ and

$$\begin{aligned} &V_i\big(\hat{x}_i^{\Delta}(t), \tilde{M}_i(t), \tilde{\mathcal{N}}_i(t), \tilde{f}_i(t), t\big) \\ &\triangleq \mathrm{tr}\left\{\Gamma_{\mathrm{M}_i}^{-1}\tilde{M}_i^{\mathrm{T}}(t)n_i^{*-1}(t)\tilde{M}_i(t)\right\} + \hat{x}_i^{\Delta^{\mathrm{T}}}(t)\hat{P}_i\hat{x}_i^{\Delta}(t) \\ &\;\; + \gamma_{\mathrm{n}_i}^{-1}n_i^{*-1}(t)\tilde{n}_i^2(t) + \gamma_{\mathrm{f}_i}^{-1}n_i^{*-1}(t)\tilde{f}_i^2(t). \end{aligned} \tag{B.5}$$

The derivative of (B.5) along the trajectories (16)–(18), (B.4) can be written as

$$\begin{aligned} &\dot{V}_i\big(\hat{x}_i^{\Delta}(t), \tilde{M}_i(t), \tilde{n}_i(t), \tilde{f}_i(t), t\big) \\ &= \hat{x}_i^{\Delta^{\mathrm{T}}}(t)[\hat{P}_i A_i^{\mathrm{d}} + A_i^{\mathrm{d}^{\mathrm{T}}}\hat{P}_i]\hat{x}_i^{\Delta}(t) \\ &\;\; + \hat{x}_i^{\Delta^{\mathrm{T}}}(t)\sum_{j\in\mathcal{N}_i}\hat{A}_{ij}\hat{x}_j^{\Delta}(t) + \sum_{j\in\mathcal{N}_i}\hat{x}_j^{\Delta^{\mathrm{T}}}(t)\hat{A}_{ij}^{\mathrm{T}}\hat{x}_i^{\Delta}(t) \\ &\;\; + 2\hat{x}_i^{\Delta^{\mathrm{T}}}(t)\hat{P}_i\hat{B}_i^{\mathrm{f}}(t)\tilde{M}_i(t)T_i^{-1}\hat{x}_i^{\Delta}(t) \\ &\;\; + 2\hat{x}_i^{\Delta^{\mathrm{T}}}(t)\hat{P}_i\hat{B}_i^{\mathrm{f}}(t)\tilde{n}_i(t)u_i^{\mathrm{c}}(t) - 2\hat{x}_i^{\Delta^{\mathrm{T}}}(t)\hat{P}_i\hat{B}_i^{\mathrm{f}}(t)\tilde{f}_i(t) \end{aligned}$$

$$
\begin{aligned}
&+2\operatorname{tr}\left\{\tilde{M}_i^{\mathrm{T}}(t)n_i^{*-1}(t)\operatorname{Proj}_{\mathrm{m}}\left[M_i(t),-B_i^{\mathrm{T}}P_ix_i^{\Delta}(t)x_i^{\Delta^{\mathrm{T}}}(t)\right]\right\}\\
&+2\tilde{n}_i(t)n_i^{*-1}(t)\operatorname{Proj}\left[n_i(t),-B_i^{\mathrm{T}}P_ix_i^{\Delta}(t)u_i^{\mathrm{c}}(t)\right]\\
&+2\tilde{f}_i(t)n_i^{*-1}(t)\operatorname{Proj}\left[\hat{f}_i(t),B_i^{\mathrm{T}}P_ix_i^{\Delta}(t)\right]\\
&-2\gamma_{\mathrm{f}_i}^{-1}\tilde{f}_i(t)n_i^{*-1}(t)\dot{f}_i(t)+\gamma_{\mathrm{f}_i}^{-1}\dot{n}_i^{*-1}(t)\tilde{f}_i^2(t)\\
&-2\operatorname{tr}\left\{\Gamma_{\mathrm{M}_i}^{-1}\tilde{M}_i^{\mathrm{T}}(t)n_i^{*-1}(t)\dot{M}_i^*(t)\right\}\\
&+\operatorname{tr}\left\{\Gamma_{\mathrm{M}_i}^{-1}\tilde{M}_i^{\mathrm{T}}(t)\dot{n}_i^{*-1}(t)\tilde{M}_i(t)\right\}\\
&-2\gamma_{\mathrm{n}_i}^{-1}\tilde{n}_i(t)n_i^{*-1}(t)\dot{n}_i^*(t)+\gamma_{\mathrm{n}_i}^{-1}\dot{n}_i^{*-1}(t)\tilde{n}_i^2(t).
\end{aligned}
\tag{B.6}
$$

Using the fact that $\operatorname{tr}\{AB\}=\operatorname{tr}\{BA\}=\operatorname{tr}\{A^{\mathrm{T}}B^{\mathrm{T}}\}$, we can conclude that

$$
\begin{aligned}
&2\hat{x}_i^{\Delta^{\mathrm{T}}}(t)\hat{P}_i\hat{B}_i^{\mathrm{f}}(t)\tilde{M}_i(t)T_i^{-1}\hat{x}_i^{\Delta}(t)\\
&\quad=2\operatorname{tr}\left\{\hat{x}_i^{\Delta^{\mathrm{T}}}(t)\hat{P}_i\hat{B}_i^{\mathrm{f}}(t)\tilde{M}_i(t)T_i^{-1}\hat{x}_i^{\Delta}(t)\right\}\\
&\quad=2\operatorname{tr}\left\{x_i^{\Delta^{\mathrm{T}}}(t)P_iB_i^{\mathrm{f}}(t)\tilde{M}_i(t)x_i^{\Delta}(t)\right\}\\
&\quad=2\operatorname{tr}\left\{\tilde{M}_i^{\mathrm{T}}(t)B_i^{\mathrm{f}^{\mathrm{T}}}(t)P_ix_i^{\Delta}(t)x_i^{\Delta^{\mathrm{T}}}(t)\right\}
\end{aligned}
\tag{B.7}
$$

Therefore,

$$
\begin{aligned}
&2\hat{x}_i^{\Delta^{\mathrm{T}}}(t)\hat{P}_i\hat{B}_i^{\mathrm{f}}(t)\tilde{M}_i(t)T_i^{-1}\hat{x}_i^{\Delta}(t)\\
&+2\operatorname{tr}\left\{\tilde{M}_i^{\mathrm{T}}(t)n_i^{*-1}(t)\operatorname{Proj}_{\mathrm{m}}\left[M_i(t),-B_i^{\mathrm{T}}P_ix_i^{\Delta}(t)x_i^{\Delta^{\mathrm{T}}}(t)\right]\right\}\\
=&\,2\operatorname{tr}\left\{\tilde{M}_i^{\mathrm{T}}(t)\left(\operatorname{Proj}_{\mathrm{m}}\left[M_i(t),-B_i^{\mathrm{f}^{\mathrm{T}}}(t)P_ix_i^{\Delta}(t)x_i^{\Delta^{\mathrm{T}}}(t)\right]\right.\right.\\
&\left.\left.+B_i^{\mathrm{f}^{\mathrm{T}}}(t)P_ix_i^{\Delta}(t)x_i^{\Delta^{\mathrm{T}}}(t)\right)\right\}
\end{aligned}
\tag{B.8}
$$

Using similar methods used in (B.7) and (B.8), we can conclude from (B.6) that

$$
\begin{aligned}
&\dot{V}_i\left(\hat{x}_i^{\Delta}(t),\tilde{M}_i(t),\tilde{n}_i(t),\tilde{f}_i(t),t\right)\\
&=\hat{x}_i^{\Delta^{\mathrm{T}}}(t)[\hat{P}_iA_i^{\mathrm{d}}+A_i^{\mathrm{d}^{\mathrm{T}}}\hat{P}_i]\hat{x}_i^{\Delta}(t)\\
&\quad+\hat{x}_i^{\Delta^{\mathrm{T}}}(t)\sum_{j\in\mathcal{N}_i}\hat{A}_{ij}\hat{x}_j^{\Delta}(t)+\sum_{j\in\mathcal{N}_i}\hat{x}_j^{\Delta^{\mathrm{T}}}(t)\hat{A}_{ij}^{\mathrm{T}}\hat{x}_i^{\Delta}(t)\\
&\quad+2\operatorname{tr}\left\{\tilde{M}_i^{\mathrm{T}}(t)\left(\operatorname{Proj}_{\mathrm{m}}\left[M_i(t),-B_i^{\mathrm{f}^{\mathrm{T}}}(t)P_ix_i^{\Delta}(t)x_i^{\Delta^{\mathrm{T}}}(t)\right]\right.\right.\\
&\quad\left.\left.+B_i^{\mathrm{f}^{\mathrm{T}}}(t)P_ix_i^{\Delta}(t)x_i^{\Delta^{\mathrm{T}}}(t)\right)\right\}\\
&\quad+2\tilde{n}_i(t)\left(\operatorname{Proj}\left[n_i(t),-B_i^{\mathrm{f}^{\mathrm{T}}}(t)P_ix_i^{\Delta}(t)u_i^{\mathrm{c}}(t)\right]\right.\\
&\quad\left.+B_i^{\mathrm{f}^{\mathrm{T}}}(t)P_ix_i^{\Delta}(t)u_i^{\mathrm{c}}(t)\right)\\
&\quad+2\tilde{f}_i(t)\left(\operatorname{Proj}\left[\hat{f}_i(t),B_i^{\mathrm{f}^{\mathrm{T}}}(t)P_ix_i^{\Delta}(t)\right]-B_i^{\mathrm{f}^{\mathrm{T}}}(t)P_ix_i^{\Delta}(t)\right)\\
&\quad-2\gamma_{\mathrm{f}_i}^{-1}\tilde{f}_i(t)n_i^{*-1}(t)\dot{f}_i(t)+\gamma_{\mathrm{f}_i}^{-1}\dot{n}_i^{*-1}(t)\tilde{f}_i^2(t)\\
&\quad-2\operatorname{tr}\left\{\Gamma_{\mathrm{M}_i}^{-1}\tilde{M}_i^{\mathrm{T}}(t)n_i^{*-1}(t)\dot{M}_i^*(t)\right\}\\
&\quad+\operatorname{tr}\left\{\Gamma_{\mathrm{M}_i}^{-1}\tilde{M}_i^{\mathrm{T}}(t)\dot{n}_i^{*-1}(t)\tilde{M}_i(t)\right\}\\
&\quad-2\gamma_{\mathrm{n}_i}^{-1}\tilde{n}_i(t)n_i^{*-1}(t)\dot{n}_i^*(t)+\gamma_{\mathrm{n}_i}^{-1}\dot{n}_i^{*-1}(t)\tilde{n}_i^2(t)
\end{aligned}
\tag{B.9}
$$

Based on Lemma 1, and the facts that $\operatorname{tr}\{AB\}\le\|A\|_{\mathrm{F}}\|B\|_{\mathrm{F}}$ and $\operatorname{tr}\{AB\}=\operatorname{tr}\{BA\}$, one can write

$$
\begin{aligned}
&\operatorname{tr}\left\{\Gamma_{\mathrm{M}_i}^{-1}\tilde{M}_i^{\mathrm{T}}(t)n_i^{*-1}(t)\dot{M}_i^*(t)\right\}\\
&\le\lambda_{\max}(\Gamma_{\mathrm{M}_i}^{-1})\operatorname{tr}\left\{n_i^{*-1}(t)\dot{M}_i^*(t)\tilde{M}_i^{\mathrm{T}}(t)\right\}\\
&\le\lambda_{\max}(\Gamma_{\mathrm{M}_i}^{-1})n_i^{*-1}(t)\|\tilde{M}_i(t)\|_{\mathrm{F}}\|\dot{M}_i^*(t)\|_{\mathrm{F}}
\end{aligned}
\tag{B.10}
$$

Using (A.2) and similar methods used in (B.10), we have

$$
\begin{aligned}
&\dot{V}_i\left(\hat{x}_i^{\Delta}(t),\tilde{M}_i(t),\tilde{n}_i(t),\tilde{f}_i(t),t\right)\\
&\le\hat{x}_i^{\Delta^{\mathrm{T}}}(t)[\hat{P}_iA_i^{\mathrm{d}}+A_i^{\mathrm{d}^{\mathrm{T}}}\hat{P}_i]\hat{x}_i^{\Delta}(t)\\
&\quad+\hat{x}_i^{\Delta^{\mathrm{T}}}(t)\sum_{j\in\mathcal{N}_i}\hat{A}_{ij}\hat{x}_j^{\Delta}(t)+\sum_{j\in\mathcal{N}_i}\hat{x}_j^{\Delta^{\mathrm{T}}}(t)\hat{A}_{ij}^{\mathrm{T}}\hat{x}_i^{\Delta}(t)\\
&\quad+2\gamma_{\mathrm{f}_i}^{-1}n_i^{*-1}(t)|\dot{f}_i(t)||f_i(t)|+\gamma_{\mathrm{f}_i}^{-1}|\dot{n}_i^{*-1}(t)||\tilde{f}_i(t)|^2\\
&\quad+2\lambda_{\max}(\Gamma_{\mathrm{M}_i}^{-1})\|\tilde{M}_i(t)\|_{\mathrm{F}}\|\dot{M}_i^*(t)\|_{\mathrm{F}}n_i^{*-1}(t)\\
&\quad+\lambda_{\max}(\Gamma_{\mathrm{M}_i}^{-1})|\dot{n}_i^{*-1}(t)|\|\tilde{M}_i(t)\|_{\mathrm{F}}^2+\gamma_{\mathrm{n}_i}^{-1}|\dot{n}_i^{*-1}(t)||\tilde{n}_i(t)|^2\\
&\quad+2\gamma_{\mathrm{n}_i}^{-1}|\tilde{n}_i(t)||\dot{n}_i^*(t)|n_i^{*-1}(t)
\end{aligned}
\tag{B.11}
$$

From Proposition 2, one can write (B.11) as

$$
\begin{aligned}
&\dot{V}_i\left(\hat{x}_i^{\Delta}(t),\tilde{M}_i(t),\tilde{n}_i(t),\tilde{f}_i(t),t\right)\\
&\le\hat{x}_i^{\Delta^{\mathrm{T}}}(t)[\hat{P}_iA_i^{\mathrm{d}}+A_i^{\mathrm{d}^{\mathrm{T}}}\hat{P}_i]\hat{x}_i^{\Delta}(t)+\hat{x}_i^{\Delta^{\mathrm{T}}}(t)\sum_{j\in\mathcal{N}_i}\hat{A}_{ij}\hat{x}_j^{\Delta}(t)\\
&\quad+\sum_{j\in\mathcal{N}_i}\hat{x}_j^{\Delta^{\mathrm{T}}}(t)\hat{A}_{ij}^{\mathrm{T}}\hat{x}_i^{\Delta}(t)+2\underline{n}_{i,\max}^*\gamma_{\mathrm{f}_i}^{-1}\tilde{f}_{i,\max}\dot{f}_{i,\max}\\
&\quad+\gamma_{\mathrm{f}_i}^{-1}\underline{\dot{n}}_{i,\max}^*\tilde{f}_{i,\max}^2+2\lambda_{\max}(\Gamma_{\mathrm{M}_i}^{-1})\underline{n}_{i,\max}^*\tilde{M}_{i,\max}\dot{M}_{i,\max}^*\\
&\quad+\lambda_{\max}(\Gamma_{\mathrm{M}_i}^{-1})\underline{\dot{n}}_{i,\max}^*\tilde{M}_{i,\max}^2+2\gamma_{\mathrm{n}_i}^{-1}\tilde{n}_{i,\max}\dot{n}_{i,\max}^*\\
&\quad+\gamma_{\mathrm{n}_i}^{-1}\underline{\dot{n}}_{i,\max}^*\tilde{n}_{i,\max}^2.
\end{aligned}
\tag{B.12}
$$

Therefore,

$$
\begin{aligned}
\dot{V}=&\sum_{i\in N}\dot{V}_i\left(\hat{x}_i^{\Delta}(t),\tilde{M}_i(t),\tilde{n}_i(t),\tilde{f}_i(t),t\right)\\
\le&-\lambda_{\min}(Q)\|\hat{x}^{\Delta}(t)\|_2^2+\sum_{i\in N}\left\{2\underline{n}_{i,\max}^*\gamma_{\mathrm{f}_i}^{-1}\tilde{f}_{i,\max}\dot{f}_{i,\max}\right.\\
&+\gamma_{\mathrm{f}_i}^{-1}\underline{\dot{n}}_{i,\max}^*\tilde{f}_{i,\max}^2+2\lambda_{\max}(\Gamma_{\mathrm{M}_i}^{-1})\underline{n}_{i,\max}^*\tilde{M}_{i,\max}\dot{M}_{i,\max}^*\\
&+\lambda_{\max}(\Gamma_{\mathrm{M}_i}^{-1})\underline{\dot{n}}_{i,\max}^*\tilde{M}_{i,\max}^2+2\gamma_{\mathrm{n}_i}^{-1}\tilde{n}_{i,\max}\dot{n}_{i,\max}^*\\
&\left.+\gamma_{\mathrm{n}_i}^{-1}\underline{\dot{n}}_{i,\max}^*\tilde{n}_{i,\max}^2\right\}.
\end{aligned}
$$

Hence, we can conclude that $\dot{V}(\cdot)<0$ outside of the compact set

$$
\begin{aligned}
\Upsilon\triangleq\Big\{&\left(\hat{x}^{\Delta},\tilde{M},\tilde{n},\tilde{f}\right)\in\mathbb{R}^{2N}\times\mathbb{R}^{2N\times2N}\times\mathbb{R}^{N}\\
&\times\mathbb{R}^{N}:\|\hat{x}^{\Delta}\|_2\le\nu,|\tilde{f}_i|\le\tilde{f}_{i,\max},\\
&\|\tilde{M}_i\|_{\mathrm{F}}\le\tilde{M}_{i,\max},|\tilde{n}_i|\le\tilde{n}_{i,\max},i=1,\dots,N\Big\},
\end{aligned}
$$

where ν is given by (20). The maximum of $V(\cdot)$ on boundary of Υ denoted by $\partial\Upsilon$ is

$$
\begin{aligned}
\alpha\triangleq&\max_{\partial\Upsilon}V\left(\hat{x}^{\Delta}(t),\tilde{M}(t),\tilde{n}(t),\tilde{f}(t),t\right)\\
=&\lambda_{\max}(\hat{P})\nu^2+\sum_{i\in N}\gamma_{\mathrm{f}_i}^{-1}\tilde{f}_{i,\max}^2+\sum_{i\in N}\lambda_{\max}(\Gamma_{\mathrm{M}_i}^{-1})\tilde{M}_{i,\max}^2\\
&+\sum_{i\in N}\gamma_{\mathrm{n}_i}^{-1}\tilde{n}_{i,\max}^2,
\end{aligned}
$$

Therefore, every trajectory of (B.4) remains inside or converges to $\Upsilon_\alpha\triangleq\left\{\left(\hat{x}^{\Delta},\tilde{M},\tilde{n}_i,\tilde{f}\right)\in\mathbb{R}^{2N}\times\mathbb{R}^{2N\times2N}\times\mathbb{R}^{N}\times\mathbb{R}^{N}:V\left(\hat{x}^{\Delta}(t),\tilde{M}(t),\tilde{n}(t),\tilde{f}(t),t\right)=\alpha\right\}$ in a finite time $\mathcal{T}$. For calculating the ultimate bound of $x^{\Delta}(t)$, note that $\Upsilon'\triangleq\left\{\left(\hat{x}^{\Delta},\tilde{M},\tilde{n}_i,\tilde{f}\right):\lambda_{\min}(\hat{P})\|\hat{x}^{\Delta}(t)\|_2^2+\sum_{i\in N}\gamma_{\mathrm{n}_i}^{-1}\underline{n}_{i,\min}^*|\tilde{n}_i(t)|^2+\sum_{i\in N}\gamma_{\mathrm{f}_i}^{-1}\underline{n}_{i,\min}^*|\tilde{f}_i(t)|^2+\sum_{i\in N}\lambda_{\min}(\Gamma_{\mathrm{M}_i}^{-1})\underline{n}_{i,\min}^*\|\tilde{M}_i(t)\|_{\mathrm{F}}^2\le\alpha\right\}$ contains Υ_α, i.e, $\Upsilon_\alpha\subset\Upsilon'$. Therefore, the bound of $\hat{x}^{\Delta}(t)$ can be calculated as $\|\hat{x}^{\Delta}(t)\|_2\le\left(\alpha/\lambda_{\min}(\hat{P})\right)^{\frac{1}{2}}$, or equivalently $\|x^{\Delta}(t)\|_2\le\left(\alpha\|T^{-1}\|_2^2/\lambda_{\min}(\hat{P})\right)^{\frac{1}{2}}$ which proves (19).

For constant additive and loss of effectiveness faults, it follows from (B.12) that $\dot{V}(\cdot)\le-\hat{x}^{\Delta\mathrm{T}}(t)Q\hat{x}^{\Delta}(t)\le0$. Using Barbalat Lemma, we can show that $\lim_{t\to\infty}x^{\Delta}(t)=0$, and the proof becomes complete. □

Appendix C. Proof of Proposition 1

Proof. We can decompose A_i^{d} given in (17) as $A_i^{\mathrm{d}}=A_0-B_0K_i$, where A_0 and B_0 are given in (22), respectively, and $K\triangleq[d_0^i,d_1^i]$. Substituting A_i^{d} in (20) and by multiply it by $\operatorname{diag}(\bar{P}^{-1},\dots,\bar{P}^{-1})$ from left and right, and using $W_i\triangleq\bar{P}^{-1}K_i^{\mathrm{T}}$, the LMI (21) can be obtained. □

References

[1] Abhishek A, Ranjan A, Devassy S, Verma BK, Ram SK, Dhakar AK. Review of hierarchical control strategies for DC microgrid. IET Renew Power Gener 2020;14(10):1631–40.

[2] Moradi M, Heydari M, Zarei SF. An overview on consensus-based distributed secondary control schemes in DC microgrids. Electr Power Syst Res 2023;225:109870.

[3] Moradi M, Heydari M, Zarei SF, Oshnoei A. Discrete-time distributed secondary control of DC microgrids with communication delays. Electr Power Syst Res 2024;226:109935.

[4] Kumar GK, Elangovan D. Review on fault-diagnosis and fault-tolerance for DC–DC converters. IET Power Electr 2020;13(1):1–13.
[5] Ortiz L, González JW, Gutierrez LB, Llanes-Santiago O. A review on control and fault-tolerant control systems of AC/DC microgrids. Heliyon 2020;6(8):e04799.
[6] Khan SS, Wen H. A comprehensive review of fault diagnosis and tolerant control in DC-DC converters for DC microgrids. IEEE Access 2021;9:80100–27.
[7] Dutta S, Sahu SK, Roy M, Dutta S. A data driven fault detection approach with an ensemble classifier based smart meter in modern distribution system. Sustain Energy, Grids Netw 2023;101012.
[8] Et-taleby A, Chaibi Y, Allouhi A, Boussetta M, Benslimane M. A combined convolutional neural network model and support vector machine technique for fault detection and classification based on electroluminescence images of photovoltaic modules. Sustain Energy, Grids Netw 2022;32:100946.
[9] Rameshrao AG, Koley E, Ghosh S. An optimal sensor location based protection scheme for DER-integrated hybrid AC/DC microgrid with reduced communication delay. Sustain Energy, Grids Netw 2022;30:100680.
[10] Jadidi S, Badihi H, Zhang Y. Passive fault-tolerant control of PWM converter in a hybrid AC/DC microgrid. In: 2019 IEEE 2nd International conference on renewable energy and power engineering (REPE). IEEE; 2019, p. 90–4.
[11] Hosseinzadeh M, Salmasi FR. Fault-tolerant power management system for a DC micro-grid in the presence of shading fault. In: Proceedings of the IEEE 24th International symposium on industrial electronics, Rio de Janeiro, Brazil. 2015, p. 3–5.
[12] Hong L, Xu Q, He Z, Ma F, Luo A, Guerrero JM. Fault-tolerant oriented hierarchical control and configuration of modular multilevel converter for shipboard MVDC system. IEEE Trans Ind Inf 2018;15(8):4525–35.
[13] Chen H, Yi H, Jiang B, Zhang K, Chen Z. Data-driven detection of hot spots in photovoltaic energy systems. IEEE Trans Syst, Man, Cybern: Syst 2019;49(8):1731–8.
[14] Huang M, Ding L, Li W, Chen C-Y, Liu Z. Distributed observer-based H_∞ fault-tolerant control for DC microgrids with sensor fault. IEEE Trans Circuits Syst I Regul Pap 2021;68(4):1659–70.
[15] Gholami S, Saha S, Aldeen M. Sensor fault tolerant control of microgrid. In: 2016 IEEE Power and energy society general meeting (PESGM). IEEE; 2016, p. 1–5.
[16] Saberi A, Salmasi FR, Najafabadi TA. Sensor fault-tolerant control of wind turbine systems. In: 2014 5th Conference on thermal power plants (CTPP). IEEE; 2014, p. 40–5.
[17] Galavizh A, Hassanabadi AH. A fuzzy fault tolerant controller design based on virtual sensor for a DC microgrid. J Comput Robot 2019;12(2):13–25.
[18] Dehkordi NM, Nekoukar V. Robust reliable fault tolerant control of islanded microgrids using augmented backstepping control. IET Gener Transm Dist 2019;14(3):432–40.
[19] Dehkordi NM, Moussavi SZ. Distributed resilient adaptive control of islanded microgrids under sensor/actuator faults. IEEE Trans Smart Grid 2019;11(3):2699–708.
[20] Ahmadi A-A, Salmasi FR, Noori-Manzar M, Najafabadi TA. Speed sensorless and sensor-fault tolerant optimal PI regulator for networked DC motor system with unknown time-delay and packet dropout. IEEE Trans Ind Electron 2013;61(2):708–17.
[21] Gholami S, Saha S, Aldeen M. Fault tolerant control of electronically coupled distributed energy resources in microgrid systems. Int J Electr Power Energy Syst 2018;95:327–40.
[22] Saha S, Roy T, Mahmud M, Haque M, Islam S. Sensor fault and cyber attack resilient operation of DC microgrids. Int J Electr Power Energy Syst 2018;99:540–54.
[23] Afshari A, Karrari M, Baghaee HR, Gharehpetian G, Karrari S. Cooperative fault-tolerant control of microgrids under switching communication topology. IEEE Trans Smart Grid 2019;11(3):1866–79.
[24] Sardashti A, Ramezani A. Fault tolerant control of islanded AC microgrids under sensor and communication link faults using online recursive reduced-order estimation. Int J Electr Power Energy Syst 2021;126:106578.
[25] Hu B, Zhou C, Tian Y-C, Hu X, Junping X. Decentralized consensus decision-making for cybersecurity protection in multimicrogrid systems. IEEE Trans Syst, Man, Cybern: Syst 2020;51(4):2187–98.
[26] Zhang Z, Dou C, Zhang B, Yue W. Voltage distributed cooperative control considering communication security in photovoltaic power system. IEEE Trans Syst, Man, Cybern: Syst 2019;49(8):1592–600.
[27] Kaiser J, Duerbaum TA. An overview of saturable inductors: Applications to power supplies. IEEE Trans Power Electron 2021;36(9):10766–75.
[28] Wu T-F, Misra M, Jhang Y-Y, Huang Y-H, Lin L-C. Direct digital control of single-phase grid-connected inverters with LCL filter based on inductance estimation model. IEEE Trans Power Electron 2018;34(2):1851–62.
[29] Mehmood F, Papadopoulos PM, Hadjidemetriou L, Polycarpou MM. Modeling of sensor faults in power electronics inverters and impact assessment on power quality. In: 2021 IEEE Madrid powertech. IEEE; 2021, p. 1–6.
[30] Zhang B, Dou C, Yue D, Zhang Z, Zhang T. A cyber-physical cooperative hierarchical control strategy for islanded microgrid facing with random communication failure. IEEE Syst J 2020;14(2):2849–60.
[31] Huang X, Li X, Wang F, Liu Y, Sun H. Short circuit detection and driving control with no blanking time for high voltage high power insulated gate bipolar transistors. IET Power Electr 2021;14(6):1138–48.
[32] Cao Q, Che Y, Yang J, Mi M, Men Y. Short-circuit and open-circuit faults monitoring of IGBTs in solid-state-transformers using collector-emitter voltage. J Power Electron 2021;21(7):1052–60.
[33] Mohsenzade S, Naghibi J, Mehran K. Reliability enhancement of power IGBTs under short-circuit fault condition using short-circuit current limiting-based technique. Energies 2021;14(21):7397.
[34] Zhang L, Chai Y, Ge X. A novel bond wires aging monitoring method of IGBT module based on the short-circuit current. In: 2021 IEEE 2nd China international youth conference on electrical engineering (CIYCEE). IEEE; 2021, p. 1–7.
[35] Wang C, Zheng Z, Wang K, Li Y. Fault detection and tolerant control of IGBT open-circuit failures in modular multilevel matrix converters. IEEE J Emerg Sel Top Power Electr 2022. http://dx.doi.org/10.1109/JESTPE.2022.3150166.
[36] Alhasnawi BN, Jasim BH, Sedhom BE. Distributed secondary consensus fault tolerant control method for voltage and frequency restoration and power sharing control in multi-agent microgrid. Int J Electr Power Energy Syst 2021;133:107251.
[37] Shahab MA, Mozafari B, Soleymani S, Dehkordi NM, Shourkaei HM, Guerrero JM. Distributed consensus-based fault tolerant control of islanded microgrids. IEEE Trans Smart Grid 2019;11(1):37–47.
[38] Ghasemi MA, Zarei SF, Peyghami S, Blaabjerg F. A theoretical concept of decoupled current control scheme for grid-connected inverter with LCL filter. Appl Sci 2021;11(14):6256.
[39] Zarei SF, Mokhtari H, Ghasemi MA, Peyghami S, Davari P, Blaabjerg F. Control of grid-following inverters under unbalanced grid conditions. IEEE Trans Energy Convers 2019;35(1):184–92.
[40] Tucci M, Riverso S, Vasquez JC, Guerrero JM, Ferrari-Trecate G. A decentralized scalable approach to voltage control of DC islanded microgrids. IEEE Trans Control Syst Technol 2016;24(6):1965–79.
[41] Tucci M, Meng L, Guerrero JM, Ferrari-Trecate G. Plug-and-play control and consensus algorithms for current sharing in DC microgrids. IFAC-PapersOnLine 2017;50(1):12440–5.
[42] Yadegar M, Afshar A, Meskin N. Fault-tolerant control of non-linear systems based on adaptive virtual actuator. IET Control Theory Appl 2017;11(9):1371–9.
[43] Yadegar M, Meskin N, Afshar A. Fault-tolerant control of linear systems using adaptive virtual actuator. Internat J Control 2019;92(8):1729–41.
[44] Yadegar M, Meskin N, Afshar A. Reconfigurable control of linear systems based on state feedback adaptive virtual actuator. In: 2017 American control conference (ACC). IEEE; 2017, p. 4123–8.
[45] Tucci M, Meng L, Guerrero JM, Ferrari-Trecate G. Consensus algorithms and plug-and-play control for current sharing in DC microgrids. 2016, arXiv:1603.03624.
[46] Yadegar M, Meskin N. Fault-tolerant control of nonlinear heterogeneous multi-agent systems. Automatica 2021;127:109514.
[47] Eugene L, Kevin W. Robust and Adaptive Control With Aerospace Applications. London: Springer; 2013.
[48] Pomet J-B, Praly L. Adaptive nonlinear regulation: estimation from the Lyapunov equation. IEEE Trans Automat Control 1992;37(6):729–40.
[49] Yadegar M, Meskin N. Fault-tolerant control of one-sided Lipschitz nonlinear systems. IEEE Control Syst Lett 2021;6:1460–5.
[50] Mori T. Comments on a matrix inequality associated with bounds on solutions of algebraic riccati and Lyapunov equation. IEEE Trans Automat Control 1988;33(11):1088.